# Effective porosity for Gassmann fluid substitution

*Fuyong Yan*, De-hua Han and Qiuliang Yao, Rock Physics Lab, University of Houston*

**Summary**

In this study, we have analyzed the complexity of pore structure and its interaction with pore fluid. The specific surface area is an important parameter related to water retention in reservoir rocks. The surface tension between mineral surface and pore fluids might be so strong that some portion of pore fluids does not respond as fluid under small pressure disturbance. Integrated study of ultrasonic lab measurement data, petrographic data, mercury injection capillary pressure (MICP) data and NMR $T_2$ data shows the rationality of using an effective porosity as input for Gassmann equation. The effective porosity for Gassmann equation should be frequency-dependent. Knowing the pore geometry, if an empirical correlation between frequency and threshold pore throat size or NMR $T_2$ is set up, Gassmann equation can be applicable to data of any frequency measurement. Without information of pore geometry, the irreducible water saturation can be used to estimate effective porosity; the "modified" Gassmann equation should give more reliable prediction of saturation effect.

**Introduction**

The Gassmann equations are widely used for fluid substitution in the industry. Although there is no pore geometry assumption in Gassmann's theory on elasticity of porous media, one of the most important assumptions is that the pore fluids reach pressure equilibrium in a representative volume(Gurevich et. Al., 2009). Pores have different sizes and shapes, and the pore walls are made of different minerals, thus the pore fluids may respond quite differently to a minor pressure disturbance. The typical strain in nondestructive ultrasonic measurement is in order of $10^{-9}$ (Rose, 1999), which means the pressure disturbance is in order of tens of Pascal for common reservoir rock. The pressure disturbance is in order of several hundreds of Pascal for seismic wave propagating in reservoir rocks if the strain is assumed to be less than $10^{-8}$. Depending on the distance to the mineral surface and type of minerals consisting of the pore wall, the surface tension on pore fluids might be so strong that some portion of pore fluids does not move like free pore fluid for the passing pressure waves. The pore throats for some pores (mostly micropores) might be too narrow for their effective communication with the macropore system. Thus to apply Gassmann equation, the porosity should be apparent or effective porosity, which is the volume fraction of pore fluids that is connected and relaxed, and the other fraction of pore fluids should be included in the rock matrix. Under this principle we can inverted the fraction of effective porosity from lab measured data. Comparing the inverted result with the pore geometry information derived from petrographic images, MICP and NMR $T_2$ can help us understand the importance of the pore geometry and have better understanding of the velocity dispersion mechanism.

**Pore geometry and pore fluid mobility**

The pore geometry we discuss here primarily refers to pore size (and its distribution) and specific surface area. Specific surface area ($S_s$) is defined as the interstitial surface area of the pores and pore channels per unit of bulk volume. It can be measured by physical absorption of gas using BET theory (Brunauer et. al., 1938). The specific surface area is primarily controlled by pore size. Pore shape and flatness of pore wall can also have significant effect on specific surface area. The parameter of specific surface area has close relation with two of the most important parameters for reservoir engineers: irreducible water saturation ($S_{wir}$) and permeability. From Figures 1 and 2, specific surface area ($S_s$) is critical in controlling irreducible water saturation and permeability.

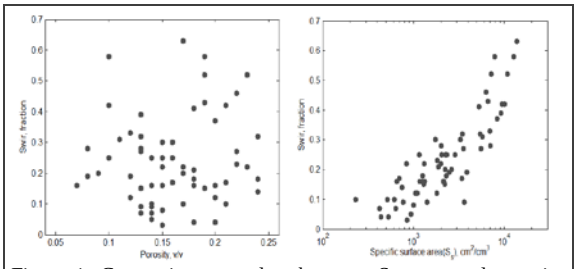


Figure 1: Comparing crossplots between $S_{wir}$ vs. total porosity and $S_{wir}$ vs. specific surface area (Data from Bagrintseva, 1977 and Chilingarian et. Al. 1990)

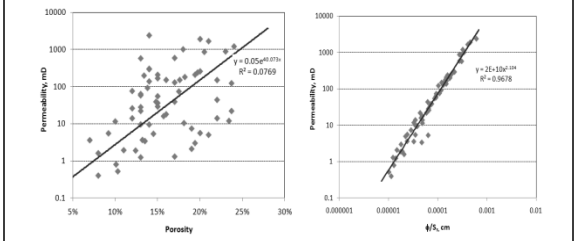


Figure 2: Comparing of crossplots between permeability vs. total porosity and permeability vs. $\phi/S_s$ (Same data source as Fig. 1)



DOI http://dx.doi.org/10.1190/segam2013-0377.1

Several mechanism of water adsorption on mineral surfaces have been proposed by Low (1961), they include hydrogen bonding, hydration of exchange cat ions, attraction by osmosis, charged surface-dipole attraction, attraction by London dispersion forces and capillary condensation. Depending on the distance of water to mineral surface, the attraction between mineral surface and water can be significant compared to the pressure disturbance caused by seismic waves in seismic exploration, which means part of the fluid will behave more like rock frame than pore fluid.

**Dual porosity Gassmann equation**

One of the most important assumptions of Gassmann theory (Gassmann, 1951) is that the pore fluids reach pressure equilibrium in a representative volume. As we analyzed above, due to complicated geometry and water-mineral surface interaction, part of the water will be adhered to the pore wall and not respond as fluid under small pressure disturbance. There are also pores that are "isolated" to the connected pore system or connected by pore throat that is too narrow and long for pressure relaxation during passing of pressure waves. These parts of pore fluids obviously do not satisfy the assumption of Gassmann's theory, and should not be counted in the pore system in the Gassmann equation. When Gassmann brought up the theory, he also gave a numerical example. In the numerical example, the sandstone has a total porosity of 17.1%, when the dry rock is saturated in water, part of the pores are inaccessible to the water, and the apparent porosity is 13.3%. To apply his theory he suggested that the apparent porosity should be used and "inaccessible" pores should be "accounted for within the solid material" (Gassmann, 1951, translated by Berryman, et. Al., 2007). So that when Gassmann brought up his theory, he had realized the pores should not necessarily be treated equally and as a whole entity.

For generality, we define all the pores that can reach pressure equilibrium in a representative volume are effective pores for Gassman's theory, and the others pores are ineffective and are accounted in the solid rock matrix. The "modified" Gassmann equation is in form of

$$\frac{K_{sat}}{K_M^{'}-K_{sat}}=\frac{K_{dry}^{'}}{K_M^{'}-K_{dry}^{'}}+\frac{K_f}{\phi_e\left(K_M^{'}-K_f\right)} \qquad (1)$$

Where $K_M'$ is the effective bulk modulus of the rock matrix including pore fluids in ineffective pores, and $K'_{\mathrm{dry}}$ is the pseudo dry bulk modulus for partially saturated rock with only ineffective pores are filled with pore fluids. The word "modified" is quoted because we believe this is more a modification than proper interpretation of Gassmann's theory.

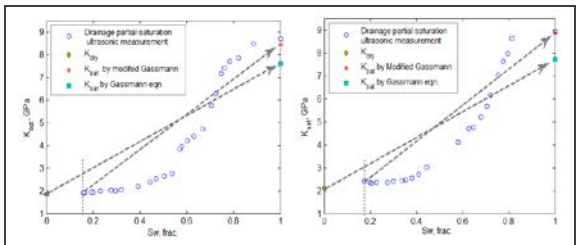


Figure 3: Comparing of saturation effect prediction using traditional Gassmann equation and "modified" Gassmann equation (The core samples are loose sandstone from Gulf of Mexico).

The pseudo dry bulk modulus is difficult to estimate since we don't know the effective porosity. Irreducible water saturation quantifies the pore fluids that cannot be driven out by hydraulic force, it might be proper to approximate the effective porosity from it.

$$\phi_e \approx \phi_t\left(1-S_{wir}\right) \qquad (2)$$

The effective bulk modulus at this saturation state is thus approximated as pseudo dry bulk modulus. Fig. 3 shows the ultrasonic measurement of partial saturation effect of two loose sandstone samples in drainage circle. The lowest water saturation point is where injection gas cannot further reduce the water saturation, and it is approximated as irreducible water saturation. Here we only consider three saturation states: dry, irreducible water saturation and 100% water saturation. We use original Gassmann equation and equations (1) respectively to predict the effective bulk modulus of 100% brine saturated rock and compare it with the measured value. For both samples, the predicted effective bulk modulus using the "modified" Gassmann equation and effective porosity is much closer to the measured value than using Gassmann equation in traditional way.

For practical application of fluid substitution on log data, we don't need to estimate the pseudo dry bulk modulus and can use equation below for fluid substitution:

$$\frac{K_{sat1}}{K_M^{'}-K_{sat1}}-\frac{K_{f1}}{\phi_e\left(K_M^{'}-K_{f1}\right)}=\frac{K_{sat2}}{K_M^{'}-K_{sat2}}-\frac{K_{f2}}{\phi_e\left(K_M^{'}-K_{f2}\right)} \qquad (3)$$

**Inversion of effective porosity from lab measurement**

We want to invert the effective porosity from lab measured data and then compare it with the pore geometry information to have better understanding of the effect of pore geometry on the saturation effect. In laboratory ultrasonic measurement, core samples are commonly measured on both room dry and fully saturated conditions. The Biot dispersion is usually negligible for consolidated



DOI http://dx.doi.org/10.1190/segam2013-0377.1

rocks, thus we can assume Gassmann equation work and use equation (1) to invert the effective porosity. The pseudo $K_{dry}$ is not measured, but we can estimate using the Hill (1963) average of $K'_M$ (the effective bulk modulus of the rock matrix including pore fluids in ineffective pores) and real $K_{dry}$. Conceptually we move all the pore fluids in ineffective pores to one side, the volume fraction of this 100% saturated section is $(\phi-\phi_e)/\phi$, and its effective bulk modulus is $K'_M$. Thus using eqn (1), the only unknown parameter $\phi_e$ can be calculated.

Fig. 4 shows the inverted fraction of effective porosity relative to total porosity using Han's data (Han, 1986) and core samples from a tight gas reservoir we recently measured. The core samples with clay content higher than 10% are not included because there might be significant non-mechanical effect during drying/saturating of the shaly sandstone(Yan and Han, 2011). From the inversion result, the fraction of effective porosity generally increases with total porosity. This is expected since the effective pores are usually macropores whose volume can be drastically reduced by diagenesis.

Although there is a general trend of decreasing fraction of effective porosity with decreasing total porosity as shown in Fig. 4, the data points are fairly scattered. Two pairs of core samples with similarly porosity are marked. The Beaver sandstone has similar (slightly higher) porosity as the Fontainebleau D sandstone, but the former has about 75% of pore spaces that are effective, while there are almost no effective pores in the Fontainebleau D sandstone. This can be explained by comparing their thin section images (right in Fig. 4). The original intergranular pores in Fontainebleau D sandstone are almost completely filled by overgrowth of quartz, there are no macropores found under optical microscope, while the intergranular macropores of sandstone are well kept for the Beaver sandstone. Similar is true for Coconino sandstone and Delaware brown sandstone. The Coconino sandstone is from a thick cross-bedded eolian deposit acting as an important regional aquifer (Weisman, 1984), its intergranuar macropores are kept much better than Delaware brown sandstone. Thus this inversion test confirm the rationality of using "modified" Gassmann to predict saturation effect.

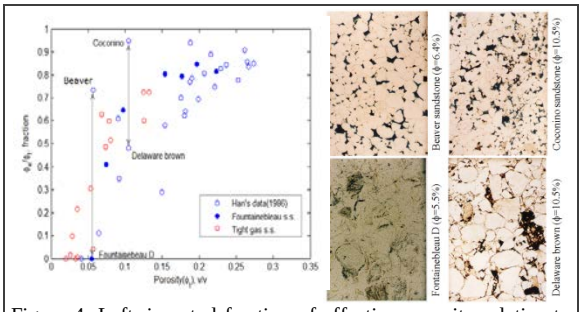


Figure 4: Left: inverted fraction of effective porosity relative to total porosity. The Fountianebleau sandstones are also from Han's data(1986). All the core samples have clay content less than 10%. Right: thin sections under plane polarized light. Except of Fontainebleau D representing an area of 0.9×1.3 $mm^2$ , the other three thin sections represent actual area of 2.2×3.2 $mm^2$ (Yale, 1984; Velasco, 1986 ). Pores are identified by dark areas with low relief.

**Pore geometry from MICP**

Mercury is a non-wetting fluid to common minerals in reservoir rocks. Driven by step-increasing pressure, mercury will preferably enter pores connected by wider pore throat. At each time the volume of mercury entered is recorded. The pore throat size under certain pressure (capillary pressure) being broken through by mercury is calculated by:

$$r_c = \frac{2\sigma\cos\theta}{P_c} \qquad (4)$$

Where σ is the interfacial tension between mercury and minerals, value of 0.480N/m is often used and the contact angle θ for mercury on minerals is often taken as 140°(Tiab and Donaldson, 2004).

The left panel of Fig. 5 shows the example of deriving pore throat size distribution from mercury injection data on one core sample. The right panel in Fig. 5 shows the pore throat radius distribution for 54 core samples from a tight sandstone gas reservoir. We also made ultrasonic velocity measurement on 16 core samples from this reservoir, under both dry and saturated conditions. Using the methodology we introduced earlier we can invert effective porosity from the laboratory measurement(Fig. 6). Since we also have information of pore size distribution of the core samples in this area, we can simply assume that there is a threshold pore throat radius, and that all pore spaces connected with pore throat wider than this threshold are effective and the other pores are ineffective. By trying different threshold pore throat radius and matching the trends of fraction of effective porosity with that inverted from ultrasonic measurement, we can estimate threshold pore throat radius under ultrasonic measurement conditions. From Fig. 6, if we assume that only pores connected by pore throat with radius wider than 36 nm are effective, obviously it is an overestimation of effective porosity; if we assume only pores connected by pore throat with radius wider than 590 nm are effective, obviously it is an underestimation of effective porosity. Best match is achieved when threshold pore throat radius of 150 nm is selected, thus the threshold pore throat size to determine effectiveness of pores under ultrasonic measurement is estimated as 150 nm.

**Pore geometry from NMR log**



DOI http://dx.doi.org/10.1190/segam2013-0377.1

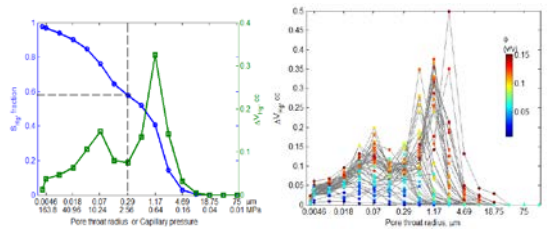

Figure 5: Mercury injection data from a tight gas sandstone reservoir. Left: Derivation of pore geometry from mercury injection data; Right: Pore throat distribution of 54 core sampels from a tight gas reservoir

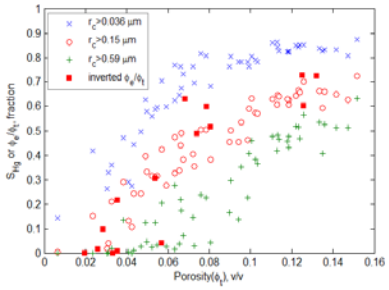


Figure 6: Estimation of threshold pore throat radius by matching effective porosity from MICP data (Fig. 5) and those inverted from ulatrasonic measurement using "modified" Gassmann equation.

NMR log measurement is based on strong response of hydrogen nucleus to external magnetic field(Coats, et. al., 1999). The pore size distribution can be estimated using either $T_1$ (longitudinal relaxation time) distribution and $T_2$ (transverse relaxation time) distribution. Overlaying the NMR $T_2$ distribution curve with pore throat size distribution curve derived from MICP, correlation between NMR $T_2$ and pore throat size can be set up (left in Fig. 7). In previous section we have estimated the threshold pore throat radius is 0.15 μm(0.30μm=300nm in diameter), from the correlation we found that the corresponding threshold NMR $T_2$ is about 10 ms, which is very close to the commonly used value of 12 ms for $T_{2cutoff}$. $T_{2cutoff}$ is a threshold value for estimation of bulk volume of irreducible water (BVI) or irreducible water saturation (right in Fig. 7). Thus the irreducible water saturation can be used to approximate the effective porosity in modified Gassmann equation for fluid substitution. This explains why the modified Gassmann equation works for the two loose sandstone core samples from Gulf of Mexico(Fig. 3).

The threshold pore throat size or $T_2$ is based on inversion of ultrasonic velocity measurement, for log data and seismic data acquired at lower frequency, it is logically that effective porosity in the "modified" Gassmann equation will increase and the threshold pore throat size or $T_2$ will decrease. If we have both reliable low frequency

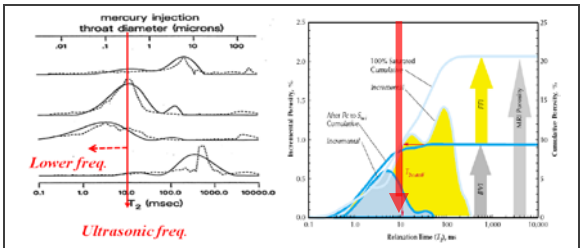


Figure 7: Left: Correlation between MICP pore throat diameter (dashed curve) and NMR T2 distribution(solid curve) by overlaying two types of curves together (after Edwards, 1999), ). The bold red arrow marks the position of the inverted threshold pore throat diameter by matching ultrasonic data and MCIP data (see Fig. 6); Right: Comparing of threshold NMR $T_2$ inverted from tight gas sandstone lab measurement with $T_{2cutoff}$ used for estiamtion of irreducible water saturation(Modified from Coates et. Al., 1999).

measurement (Batzle, et. al. 2006) and information about the pore throat size distribution or $T_2$ distribution of the sample, we can determine effective porosity for different frequency and set up an empirical correlation between frequency and threshold pore throat size or NMR $T_2$. For practical application of fluid substitution on log, if we have NMR log data, we can using the correlation between frequency and threshold $T_2$ to construct a log curve of effective porosity for more reliable prediction of saturation effect.

## Conclusions

We suggest that effective instead of total porosity should be used in the Gassmann equation. Integrated study of ultrasonic lab measurement data, petrographic data, MICP data and NMR $T_2$ data shows the rationality of the "modified" Gassmann equation. The effective porosity of a reservoir rock for the "modified" Gassmann equation should vary with the frequency. Knowing the pore geometry, if we set up a correlation between frequency and threshold pore throat size or NMR $T_2$, Gassmann equation can be applicable to any frequency measurement. Without information of pore geometry, the irreducible water saturation can be used to approximate the effective porosity; the "modified" Gassmann equation should give more reliable prediction of saturation effect in the same frequency range.

## Acknowledgement

Special thanks are Huizhu Zhao for the lab measurement. We would also like to thank the Fluid/DHI consortium sponsors for supporting the consortium and this study





DOI http://dx.doi.org/10.1190/segam2013-0377.1

http://dx.doi.org/10.1190/segam2013-0377.1

**EDITED REFERENCES**

Note: This reference list is a copy-edited version of the reference list submitted by the author. Reference lists for the 2013 SEG Technical Program Expanded Abstracts have been copy edited so that references provided with the online metadata for each paper will achieve a high degree of linking to cited sources that appear on the Web.

**REFERENCES**

Bagrinsterva, K. I., 1977, Carbonate rocks – Oil and gas reservoirs: Nedra Press.

Batzle, M. L., D.-H. Han, and R. Hofmann, 2006, Fluid mobility and frequency-dependent seismicity velocity – Direct measurements: Geophysics, **71**, no. 1, N1–N9, http://dx.doi.org/10.1190/1.2159053.

Brunauer, S., P. H. Emmett, and E. Teller, 1938, Adsorption of gases in multimolecular layers: Journal of the American Chemical Society, **60**, no. 2, 309–319, http://dx.doi.org/10.1021/ja01269a023.

Chilingarian, G. V., J. Chang, and K. I. Bagrintseva, 1990, Empirical expression of permeability in terms of porosity, specific surface area, and residual water saturation of carbonate rocks: Journal of Petroleum Science Engineering, **4**, no. 4, 317–322.

Coates, G. R., L. Xiao, and M. G. Prammer, 1999, NMR logging principles and applications: Halliburton Energy Services Publication.

Edwards, G. M., 1999, NMR imaging of fluids and flow in porous media: Methods in the Physics of Porous Media, **35**.

Gassmann, F., 1951, On elasticity of porous media: Classics of elastic wave theory: SEG.

Gurevich, B., M. Brajanovsk, R. J. Galvin, T. M. Muller, and J. Toms-Steward, 2009, P-wave dispersion and attenuation in fractured and porous reservoirs —Poroelasticity approach: Geophysical Prospecting, **57**, no. 2, 228, http://dx.doi.org/10.1111/j.1365-2478.2009.00785.x.

Han, D.-H., 1986, Effects of porosity and clay content on acoustic properties of sandstones and consolidated sediments: Ph.D. thesis, Stanford University.

Hill, R., 1963, Elastic properties of reinforced solid: Some theoretical principles: Journal of the Mechanics and Physics of Solids, **11**, no. 5, 357–372, http://dx.doi.org/10.1016/0022-5096(63)90036-X.

Low, P. F., 1961, Physical chemistry of clay-water interaction: Advances in Agronomy, **13**, 269–327, http://dx.doi.org/10.1016/S0065-2113(08)60962-1.

Rose, J. L., 1999, Ultrasonic waves in solid media: Cambridge University Press.

Tiab, D., and E. C. Donaldson, 2004, Petrophysics: Theory and practice of measuring reservoir rock and fluid transport properties, 2nd ed.: Elsevier Inc.

Velasco, K. K., 1986, Rock catalog: Stanford rock physics: Stanford University.

Weisman, M. C., 1984, Geology of the pine and northern Buckhead Mesa quadrangles, Mogollon Rim region, central Arizona: M. S. thesis, Northern Arizona University.

Yale, L. B., 1984, Rock catalog: Stanford rock physics: Stanford University.

Yan, F., and D.-H. Han, 2011, Theoretical validation of fluid substitution by Hashin-Schtrikman bounds: Presented at the 81st Annual International Meeting, SEG.